



Silver Nanoparticle-Decorated Tin Oxide Thin Films: Synthesis, Characterization, and Hydrogen Gas Sensing

Amar K. Mohamedkhair^{1,2}, Q. A. Drmosh² and Zain H. Yamani^{1,2*}

¹ Physics Department, King Fahd University of Petroleum and Minerals, Dhahran, Saudi Arabia, ² Center of Research Excellence in Nanotechnology, King Fahd University of Petroleum and Minerals, Dhahran, Saudi Arabia

OPEN ACCESS

Edited by:

Kalisadhan Mukherjee,
Pandit Deendayal Petroleum
University, India

Reviewed by:

Tarapada Sarkar,
University of Maryland, College Park,
United States
Subhasis Roy,
University of Calcutta, India

*Correspondence:

Zain H. Yamani
zhyamani@kfupm.edu.sa

Specialty section:

This article was submitted to
Functional Ceramics,
a section of the journal
Frontiers in Materials

Received: 20 June 2019

Accepted: 24 July 2019

Published: 16 August 2019

Citation:

Mohamedkhair AK, Drmosh QA and
Yamani ZH (2019) Silver
Nanoparticle-Decorated Tin Oxide
Thin Films: Synthesis,
Characterization, and Hydrogen Gas
Sensing. *Front. Mater.* 6:188.
doi: 10.3389/fmats.2019.00188

In this work, sputtered tin oxide films, decorated with silver nanoparticles were fabricated as hydrogen sensors. The fabricated thin films were characterized for their structural, compositional, morphological properties using various characterization techniques including X-ray photoelectron spectroscopy, UV-Vis absorption, X-ray diffraction, field emission scanning electron microscope, and atomic force microscopy. The morphological characterization confirmed the formation of nanoparticle-decorated SnO₂ thin films. X-ray photoelectron spectroscopy analysis established the presence of silver/silver oxide on SnO₂ thin films. The gas sensing properties of the fabricated sensors were investigated at different concentrations of hydrogen gas, over an operating temperature range of room temperature to 500°C. It was found that the prepared sensor can detect a low hydrogen concentration (50 ppm) at high operation temperature, while the higher concentration (starting from 600 ppm) can be detected even at room temperature. Furthermore, on the basis of the electronic interaction between the SnO₂ and the Ag nanoparticles, we propose a reaction model to explain the qualitative findings of the study.

Keywords: tin oxide, silver, silver oxide, thin film, gas sensor, hydrogen

INTRODUCTION

Intense research is ongoing for green “future fuel” due to its extraordinary abilities including availability in the natural resources and zero CO₂ emission (Crabtree et al., 2004). Since hydrogen (H₂) has these characteristics, research is taking place in order to produce H₂-fueled engines, in order to reduce atmospheric pollution and harmful emissions (Crabtree et al., 2004; Pal and Agarwal, 2018; Tsujimura and Suzuki, 2019). In addition, H₂ is used in petrochemical processes, including the hydrocracking process (Lippke et al., 2018) for example.

H₂ is tasteless, colorless, and odorless. With a very low ignition energy of 0.02 mJ, it inflames easily in the air at volume concentrations ranging from 4 to 75%. Therefore, detecting H₂ by a proper sensor prevents the threat of fire and explosions. So far, several different types of H₂ sensors have been established such as optical fibers (Wu et al., 2018) and surface acoustic wave (D’amico et al., 1982). Metal oxide sensors (Moseley, 1997) have been widely studied as H₂ sensors due to their excellent qualities in terms of low cost, high sensitivity, fast response, and compact size. Furthermore, their non-stoichiometric nature allows them to absorb the ambient oxygen and

exchange electrons during the adsorption and desorption processes. However, these metal oxide gas sensors have some limitations such as their inability to detect extremely low concentrations of the target gas and their requirement to operate at high temperatures. This usually puts restrictions on their portability.

Currently, a lot of research focuses on improving the sensing features of the metal oxide gas sensors. Doping of the metal oxide sensors with noble metal nanoparticles is a powerful method that improves selectivity and sensitivity, even at low operation temperatures (Kohl, 1990; Ippolito et al., 2005). Among the various metal oxide sensors, tin oxide (SnO_2), which is an n-type semiconductor, is one of the most promising materials for gas sensing applications, and especially for H_2 detection. H_2 sensors based on SnO_2 nanowires, nanorods, and nanotubes have good sensitivity, but they are still unsuitable for commercial purposes due to limitations in their fabrication techniques (Van Duy et al., 2012). Indeed, for commercialization purposes, thin films are the most investigated gas sensor nanostructures due to their simplicity in configuration and scalability of fabrication. As sensitivity is one of the most important parameters in H_2 gas sensing, many efforts have been made to enhance the sensitivity of the SnO_2 thin-film sensors. The decoration of SnO_2 with noble metals leads to charge transfer between their two surfaces, hence modifying the Fermi level of the metal oxide and affecting the charge depletion layer. This leads to increasing the electrons in the metal oxide conduction band, which in turn increases the surface interaction between the sensor and the ambient oxygen, and hence enhancing the performance of the sensor.

Korotcenkov et al. (2007) reported that by doping SnO_2 with Pd, both response time and sensitivity to CO and H_2 increase. Kocemba and Rynkowski (2011), in addition, noticed that sputtered SnO_2 thin-film doping with Pt as a catalyst gives a high sensitivity to H_2 as a function of different operating temperatures. Chen et al. (2011) reported that the synthesis of SnO_2 and Ag_2O nanocomposites demonstrate an enhancement in their gas sensing properties. Wu et al. (2013) formed Ag/ SnO_2 core shells and noticed an improvement in the sensor response to ethanol at room temperature.

For improved H_2 gas sensing properties, such as higher sensing and stability capabilities, we have developed an H_2 sensor using catalytic particles (a noble metal loading). In particular, we decorated the surface of sputtered SnO_2 thin films with Ag nanoparticles. More specifically, to maximize the catalytic effect of the sensor, the Ag nanoparticles were homogeneously decorated, covering the whole area of the surface of SnO_2 thin films through a new synthetic method. The details about H_2 -gas sensing mechanism are discussed in the results section.

EXPERIMENTAL

Synthesis of Ag Nanoparticle-Decorated SnO_2 Thin Films

Three steps were used to prepare Ag nanoparticle-decorated SnO_2 thin films for fabricating H_2 sensors. Firstly, a target of 99.995% SnO_2 (purchased from ACI Alloys INC) was utilized to fabricate SnO_2 thin films using the RF sputtering technique (model NSC-4000, Nanomaster). Before deposition

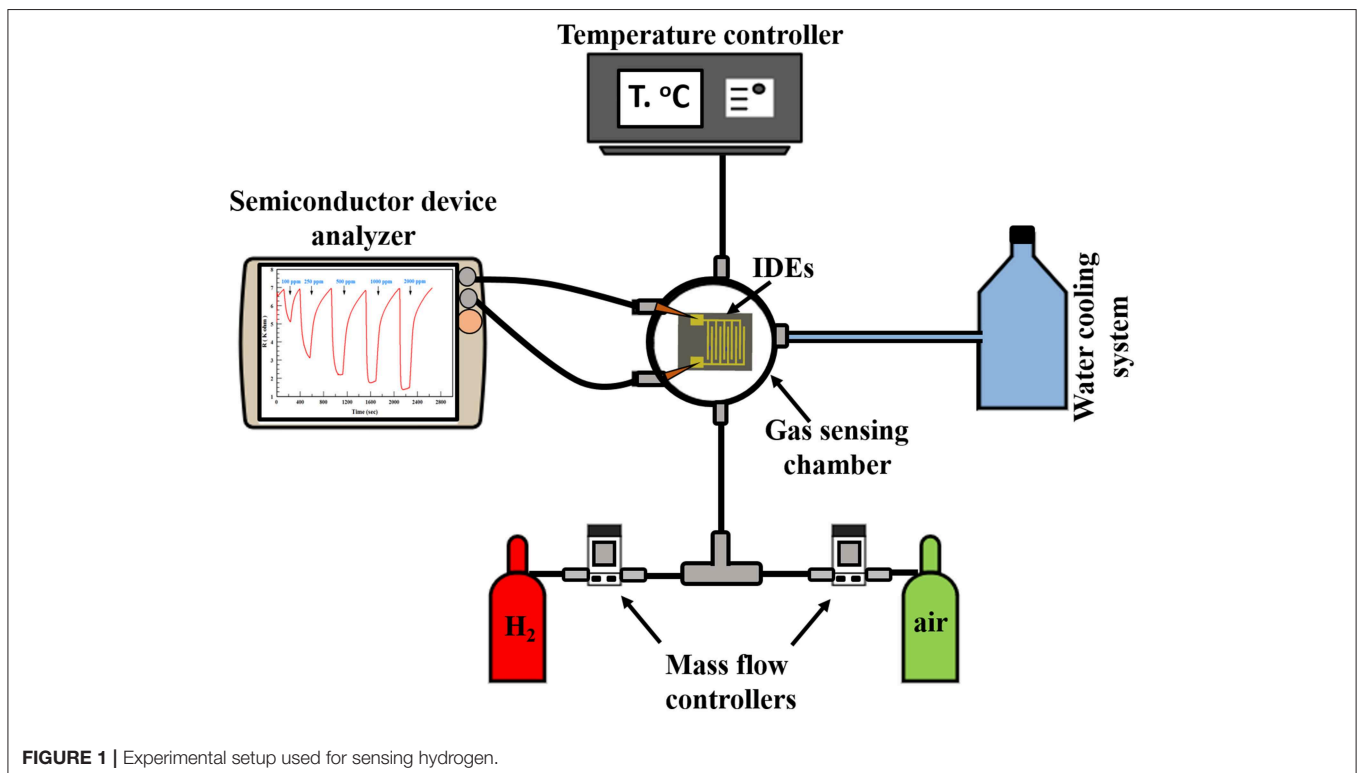
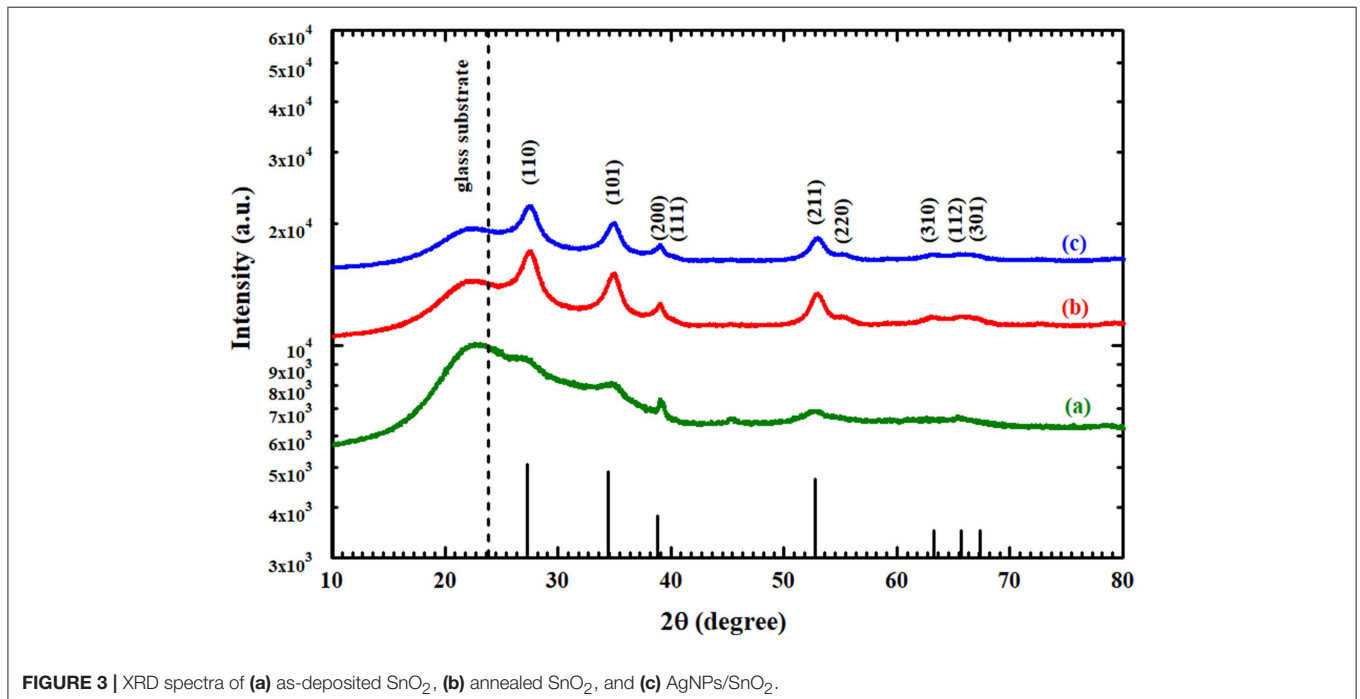
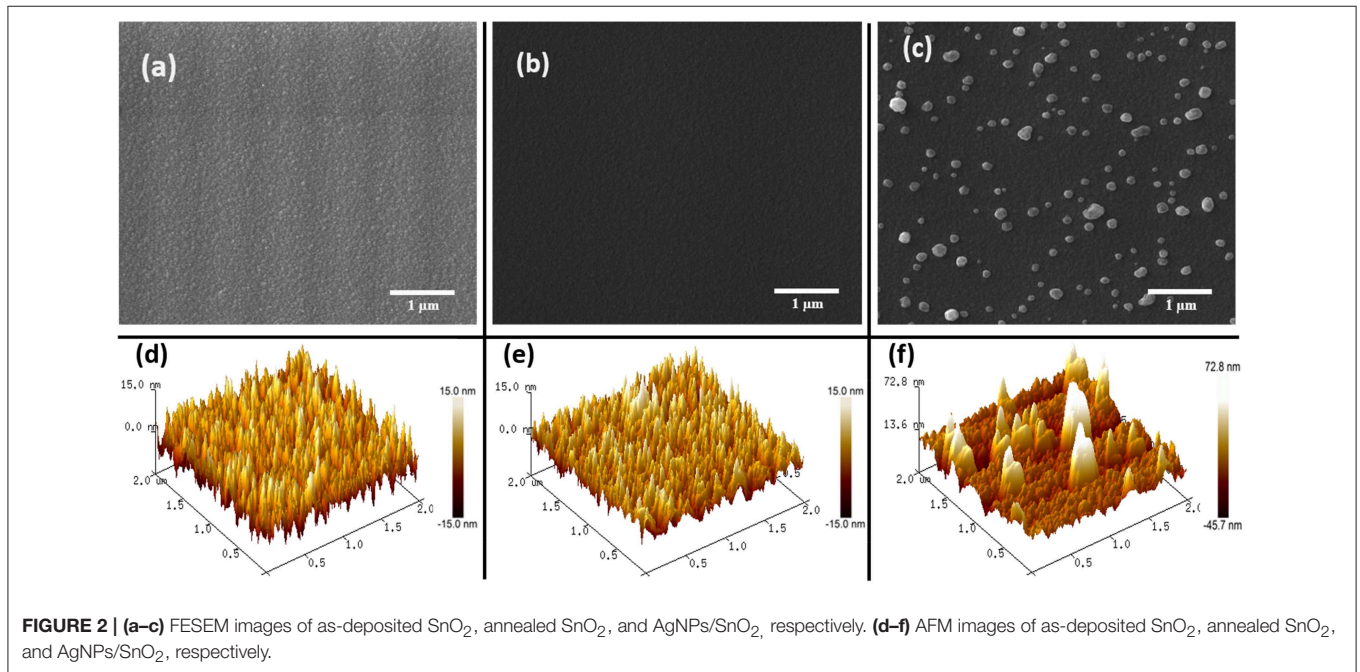


FIGURE 1 | Experimental setup used for sensing hydrogen.

of the thin films, the deposition chamber and targets were cleaned with acetone and isopropanol while the substrates were sonicated in ethanol for 30 min. For sputtering deposition, the base pressure and deposition pressure were adjusted at 6×10^{-6} and 4.8×10^{-3} torr, respectively. The SnO_2 thin films with 250 nm thickness were deposited at 60 standard cubic centimeters per minute (sccm) argon and 10 sccm oxygen gas flow rate using 100 W RF sputtering power for 120 min. The

film was deposited on SiO_2 substrates with pre-interdigitized Au electrodes (IDEs) to be used as hydrogen gas sensor, and also deposited on glass substrate to study the structural, compositional, morphological, and optical characterization of the fabricated films. The IDEs have 22 electrodes that are 200 nm thick, with 250 μm interspacing distance, connected to two pads used for electrical measurements. Secondly, a metallic target of 99.995% Ag (purchased from Semiconductor wafer) was used



to deposit a thin layer of Ag using 20 W DC sputtering power for 30 s. The Ar flow was kept at 70 sccm during the Ag layer deposition. Finally, the obtained thin films were heated at 600°C in a sealed tubular furnace (OTF-1200X from MTI corp.) with a temperature ramp rate of 20°C/min in a flowing argon atmosphere for 2 h to convert Ag layer into nanoparticles in the case of the Ag nanoparticle-decorated SnO₂ film and to enhance the crystallinity and stabilize the based SnO₂ deposited film for both pure SnO₂ film (termed as annealed SnO₂) and Ag nanoparticle-decorated SnO₂ film (termed as AgNPs/SnO₂). In addition to these two samples, one sample was left as-deposited (termed as as-deposited SnO₂) in order to study the effect of the annealing process.

Characterization

The synthesized thin films were characterized using different techniques. X-ray diffraction [Rigaku Miniflex 600 X-Ray Diffraction (XRD), with Cu K irradiation at $\lambda = 1.5406 \text{ \AA}$] was used to examine the crystalline phases, lattice parameter, and the crystalline size. X-ray photoelectron spectroscopy (Model: ESCALAB250Xi, XPS) was utilized to determine the chemical composition of the fabricated thin films. The structural morphology was investigated using a field-emission scanning electron microscope (FE-SEM; Tescan Lyra 3) and atomic force microscopy (AFM; Dimension Icon, Bruker). Optical transmittance and optical band gap measurements were carried out using double beam UV/Vis spectrophotometer (Jasco V-570) in the wavelength range of 200–1,400 nm.

Gas Sensing Measurements

The H₂ sensing measurements of the thin-film sensors were conducted by a flow-through technique. The measurement system consists of a gas sensing chamber (Linkam stage, Model HFS-600E-PB4, UK). It contains two metal needles as electrical connections between the IDE pads (i.e., the sensor) and the electrical measurement setup. In addition, the Linkam stage involves a heating unit that has the ability to reach up to 600°C. A mass flow controller (MFC, Horiba, USA) was utilized to control the gas injection into the testing chamber. The sensor resistance was measured through an Agilent B1500A Semiconductor Device Analyzer (SDA) using I/V-t measurements. Dry air, from a cylinder, was used as the background reference gas. H₂ gas cylinder (1% H₂-bal. N₂) was used as the test-gas source. The resistance across the IDE pads would change depending on the H₂ concentration changing inside the Linkam stage. The gas sensing system layout is shown in Figure 1.

RESULTS AND DISCUSSION

Structure, Morphology, and Composition Test

FE-SEM and AFM imaging techniques were used to investigate the morphological properties of the fabricated thin films. Figures 2a,b shows the FE-SEM micrograph of the as-deposited SnO₂ and the annealed SnO₂ thin films. Both micrographs show the uniformity of the SnO₂ thin film though there seems to be

a slight difference in the roughness of SnO₂ surface before and after the annealing. Figure 2c displays the annealed AgNPs/SnO₂ films at 600°C. The Ag nanoparticles were nearly uniformly distributed over the SnO₂ film surface with different particle sizes (Drmosh et al., 2015).

Figures 2d,e are 2 $\mu\text{m} \times 2 \mu\text{m}$ AFM topography images of the as-deposited SnO₂ and annealed SnO₂ thin films. As presented by SEM, the AFM images show a rough surface for the pristine film, and a more mild roughness for the film after annealing. This accentuates that annealing the SnO₂ thin film makes it denser and smoother. This is a result of the film obtaining sufficient energy from the annealing process enabling the atoms to rearrange their position, and hence become closer packed and crystalline (Shinde et al., 2005), as confirmed below by the XRD results. The AFM image of the AgNPs/SnO₂ film (Figure 2f) shows the growth of large, separated, and spaced Ag particles over the smooth SnO₂. The AgNPs size ranged approximately from 50 to 250 nm.

Figure 3 shows the XRD patterns of the pure SnO₂ thin film before and after the heat treatment and the annealed AgNPs/SnO₂. The wide peaks that appear at $\sim 24^\circ\text{C}$ correspond to the substrate (Chakraborty et al., 2010). All XRD peaks identify the standard crystal planes of tetragonal SnO₂ (Ansari

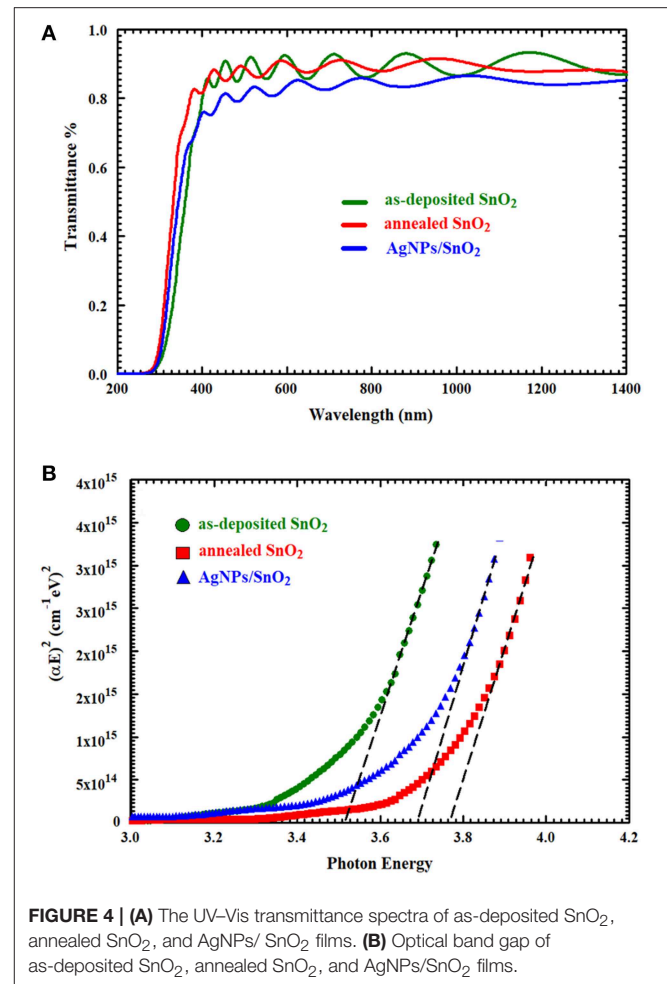


FIGURE 4 | (A) The UV-Vis transmittance spectra of as-deposited SnO₂, annealed SnO₂, and AgNPs/SnO₂ films. **(B)** Optical band gap of as-deposited SnO₂, annealed SnO₂, and AgNPs/SnO₂ films.

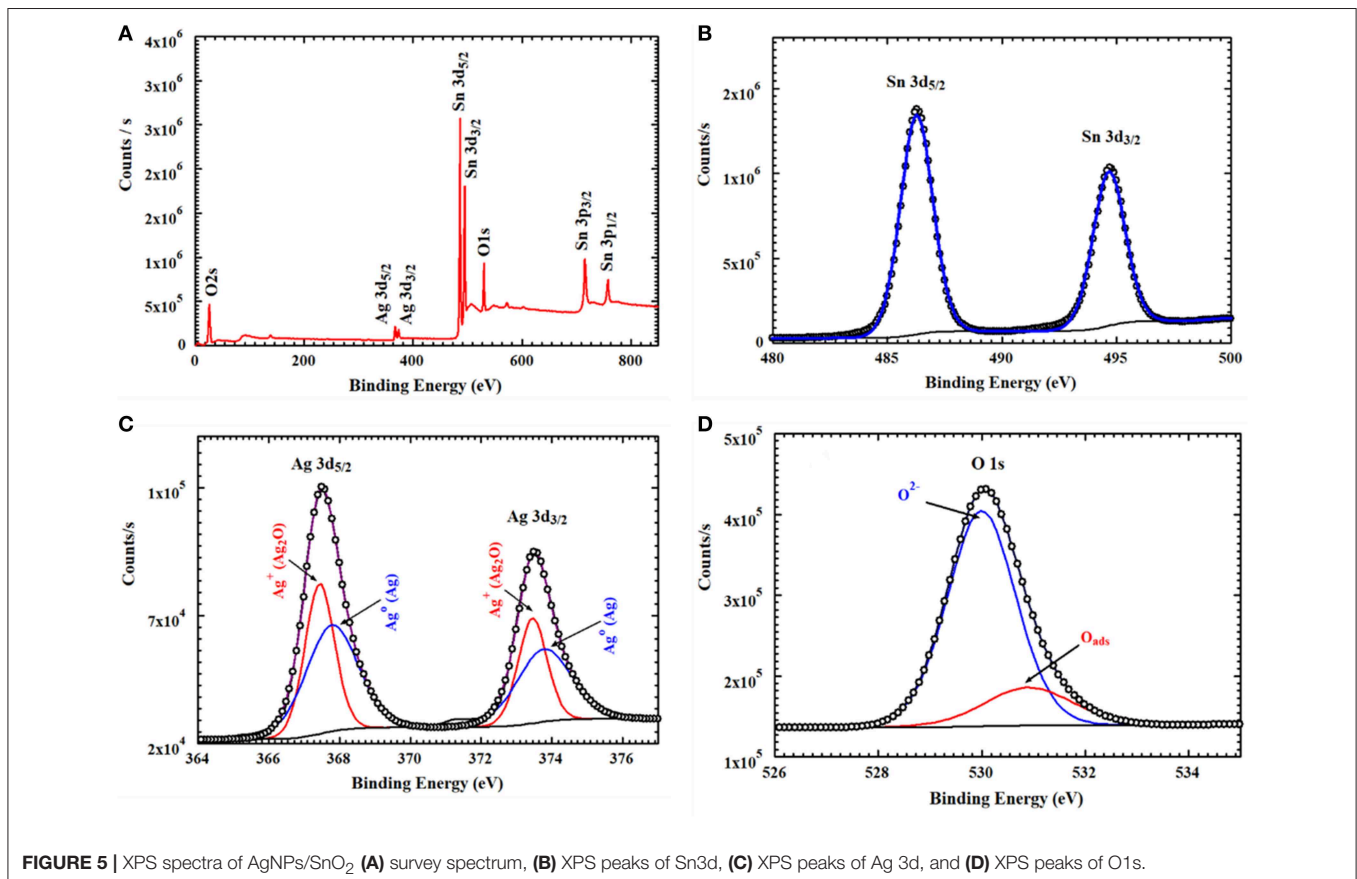
et al., 1997). From **Figure 3a**, the observed low and wide peaks correspond to the diffractions peaks (110), (101), and (200) (Ansari et al., 1997). This confirms the amorphous nature of the as-deposited SnO₂. After heating the as-deposited SnO₂ to 600°C, it is observed that the peaks become sharper, as displayed in **Figure 3b**. This is attributed to the transformation of the SnO₂ from an amorphous to a polycrystalline structure. No diffraction peaks were found related to Ag nanoparticles as there is no change in the diffraction pattern between **Figures 3a,c**. This might be due to the random distribution and low concentration of Ag nanoparticles at the surface of the SnO₂ film (Yang et al., 2014). No impurity peaks or other phases were observed, confirming the purity of the prepared films.

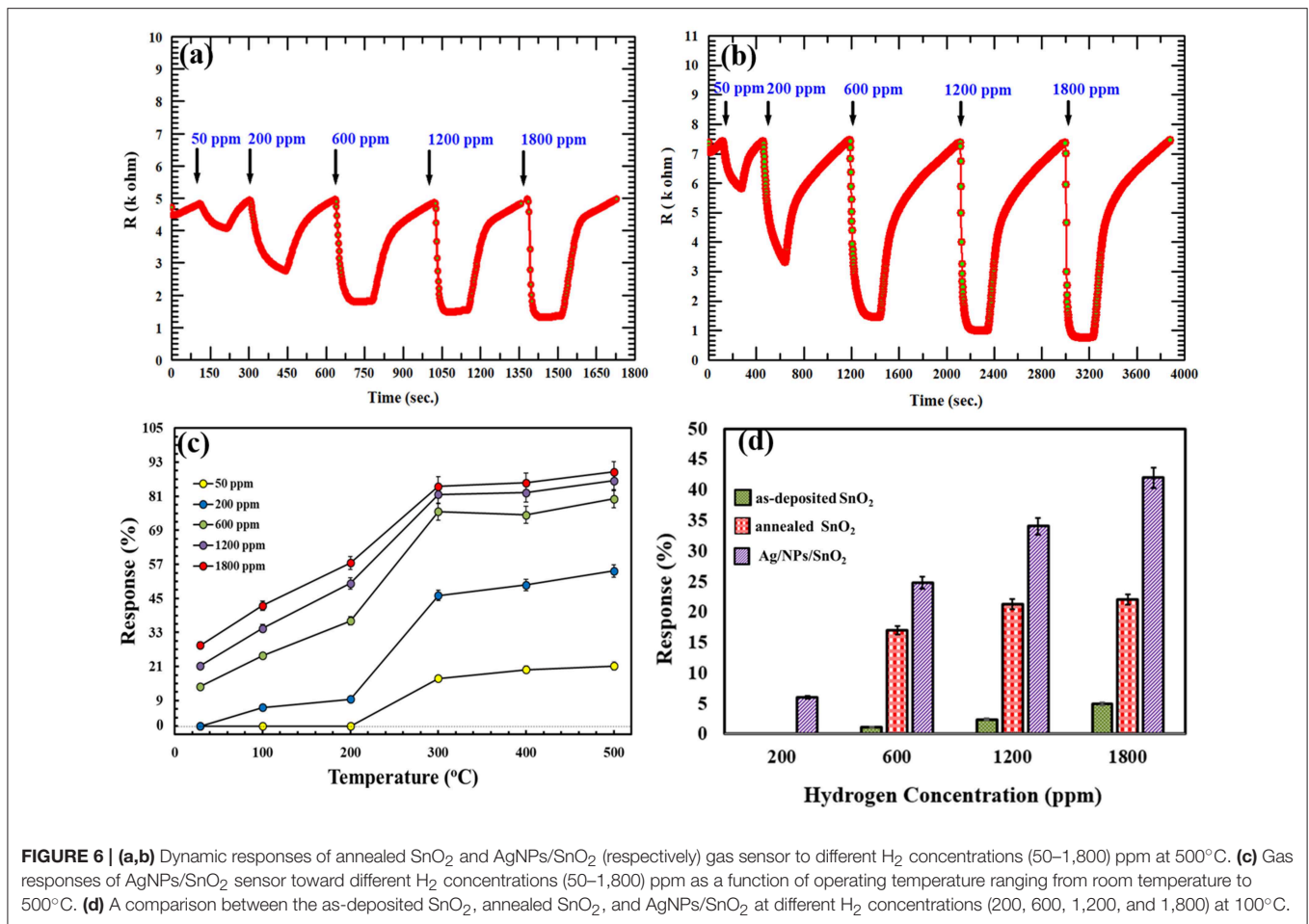
UV-Vis spectra of the synthesized thin films were obtained within a wavelength range of 200–1,400 nm, as shown in **Figure 4A**. In the IR and visible region, the optical transmittance fluctuated due to the interference of light being sandwiched inside the thin film between the substrate and air (Cho, 2014). It can be observed that the transmittance of the AgNPs/SnO₂ slightly decreased below the pure and annealed SnO₂. Certainly, this is attributed to the existence of Ag nanoparticles on the SnO₂ surface (Dasgupta et al., 2010) which has considerable absorption to electromagnetic radiation. Tauc relation $(\alpha E)^2 = A(E - E_g)$ was used to calculate the optical band gap of these films by plotting the values of $(\alpha E)^2$ against E and extrapolating the linear portion of the curves, where E and E_g are the photon

energy of incident light and optical band gap, respectively, A is a constant, and α is the absorption coefficient (Kumar et al., 1999). As can be seen from the extrapolation in **Figure 4B**, the optical band gap of the both annealed SnO₂ and AgNPs/SnO₂ increased in comparison with the as-deposited SnO₂ sample, and hence, the absorption edge was shifted to shorter wavelength as

TABLE 1 | Surface element composition of the as-deposited SnO₂, annealed SnO₂, and AgNPs/SnO₂.

Name	Sample	Peak binding energy (eV)	FWHM (eV)	Area ($\times 10^3$)	Atomic %
Sn3d	As-deposited SnO ₂	483.9	2.37	85	3.4
		485.9	1.62	2425	96.6
	Annealed SnO ₂	485.8	1.66	1508	100
	AgNPs/SnO ₂	486.3	1.63	2303	100
O1s	As-deposited SnO ₂	529.6	1.51	448	78.1
		530.4	1.92	126	21.9
	Annealed SnO ₂	529.6	1.53	447	77.1
	AgNPs/SnO ₂	530.4	2.03	133	22.9
	AgNPs/SnO ₂	530.0	1.56	449	81.5
	AgNPs/SnO ₂	530.9	2.01	102	18.5
Ag3d	AgNPs/SnO ₂	367.4	1.06	62	44.4
		368.0	1.47	42766	55.6





shown in **Figure 4A** (Reddy et al., 2013). As an effect of the annealing process, the Ag diffuses into the SnO₂ crystal. As a result, the band gap of the Ag/NPs/SnO₂ sample is smaller than the annealed SnO₂ (Hwang et al., 2011).

XPS analysis provided information about the thin film's composition. It also determined the oxidation states of the elements. From example, **Figure 5** relates to the annealed AgNPs/SnO₂ sample. The survey scan (**Figure 5A**) confirms the presence of the Sn 3d, O 1s, and the Ag 3d. The binding energy and atomic ratio of each element are demonstrated in **Table 1**. **Figure 5B** shows two peaks in the range from 483 to 489 eV and from 492 to 498 eV. These relate to the binding energies of the Sn 3d_{5/2} and Sn 3d_{3/2}, respectively (Wang et al., 2005). **Figure 5C** shows the Ag 3d_{5/2} and Ag 3d_{3/2} located in the range of 365 to 370 eV and 372 to 376 eV, respectively. In each of the two peaks, two Ag oxidation states are identified; the Ag⁰ peaks are centered at 367.8 and 373.8 eV, while the Ag⁺ peaks are centered at 367.5 and 373.4 eV (Zielinska et al., 2010). The Ag⁺ peak is due to the presence of the Ag₂O layer on top of Ag nanoparticles that are exposed to ambient oxygen (Matsushima et al., 1988). The O 1s spectrum is shown in **Figure 5D**. The convolution peak centered at 529.9 eV is ascribed to surface lattice oxygen O₂⁻, while the O_{ads} peak, centered at 530.8 eV, is

attributed to water species adsorbed on the surface of the film (Wang et al., 2016).

Gas Sensing Studies

The gas sensing performance of the AgNPs/SnO₂ thin film was tested toward H₂, and the results were compared with that of the annealed SnO₂. **Figures 6a,b** shows the response of annealed SnO₂ and AgNPs/SnO₂ for different H₂ concentrations (50–1,800 ppm) at 500°C operation temperature. The comparison of H₂ sensing performance of the two sensors reveals that addition of Ag nanoparticles to the SnO₂ thin film results in a remarkable enhancement in the sensitivity of the sensor. For example, the response of the SnO₂ decorated by Ag toward 50 ppm of H₂ is around 21% while that for pure SnO₂ is 14%. That is, Ag decoration improved the sensitivity by about 67%.

The synthesized Ag-decorated sensor was studied at wide range of operating temperatures starting from room temperature (RT = 29°C) and up to 500°C as shown in **Figure 6c**. For low concentrations (i.e., 50 and 200 ppm), the film showed no response at RT and only a small response at 100 and 200°C for 200 ppm. At higher concentrations (600, 1,200, and 1,800 ppm), the films gave an acceptable response at RT, with the response increasing by increasing the operating temperature to 500°C.

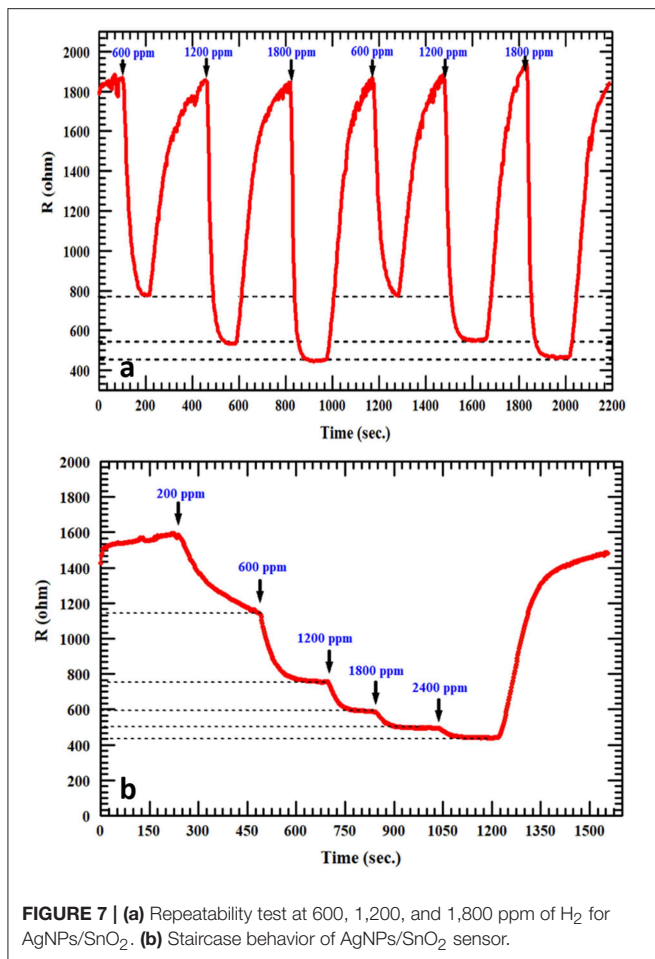


FIGURE 7 | (a) Repeatability test at 600, 1,200, and 1,800 ppm of H₂ for AgNPs/SnO₂. (b) Staircase behavior of AgNPs/SnO₂ sensor.

Figure 6d shows the comparison between the as-deposited SnO₂, annealed SnO₂, and AgNPs/SnO₂ sensors toward various H₂ concentrations (200–1,800 ppm) at low operation temperature (100°C). The annealed AgNPs/SnO₂ sensor exhibits higher response for all H₂ concentrations. For example, at 1,800 ppm, the response of as-deposited and annealed SnO₂ was ~6 and ~20%, respectively, while the response reached ~42% from the AgNPs/SnO₂ sensor. On the other hand, at low concentration (200 ppm), both as-deposited and annealed SnO₂ had no response and yet AgNPs/SnO₂ gave an acceptable response of ~7%, which confirms the value of using Ag to boost the sensitivity of the hydrogen sensor.

The reproducibility of measurements was tested in order to study the stability of the AgNPs/SnO₂ sensor, which is one of the vital properties for H₂ sensors. **Figure 7a** shows that two cycles of three different concentrations (600, 1,200, and 1,800 ppm) were used in this test. Clearly, the sensor has the ability to recover to the same initial response (600 ppm) after introducing different amounts of H₂ concentrations (1,200, 1,800 ppm), which confirms the stability of the fabricated sensor. The staircase behavior was also obtained, as shown in **Figure 7b**. The AgNPs/SnO₂ sensor

TABLE 2 | A comparison between the fabricated AgNPs/SnO₂ sensor with the different sensors reported in the literature.

Sensor	Optimum operation temperature	Response	H ₂ concentration (ppm)	References
Co/SnO ₂	175	47.2 ^a	1,000	Zhang et al., 2019
Polyaniline/SnO ₂	30	42 ^a	6,000	Sonwane et al., 2019
SnO ₂ @rGO	80	1.58 ^b	1,000	Ren et al., 2018
SnO ₂	150	5.5 ^a	1,000	Shen et al., 2015
SnO ₂ /Au-SiO ₂	100	11.5 ^b	1,000	El-Maghraby et al., 2013
CNT/SnO ₂	350	95 ^c	40,000	Majumdar et al., 2014
Pd-SnO ₂ /MoS ₂	RT	8 ^c	1,000	Zhang et al., 2017
Pt-loaded SnO ₂	200	10 ^a	1,000	Liewhiran et al., 2014
Ce doped SnO ₂	200	80 ^c	500	Deivasegamani et al., 2017
Er-doped SnO ₂	360	28 ^a	100	Singh and Singh, 2019
AgNPs/SnO ₂	300	80 ^c	600	This work

$$a: \text{response} = \frac{R_a}{R_g}, \quad b: \text{response} = \frac{R_a - R_g}{R_g} \times 100, \quad c = \frac{R_a - R_g}{R_a} \times 100.$$

shows excellent resistance descending mode from 200 to 2,400 ppm besides its ability to recover the initial resistance level, as it should for a stable sensor, when decreasing the concentration back to 200 ppm. **Table 2** compares the H₂ sensing properties of the fabricated AgNPs/SnO₂ sensor with the different sensors, operating in the dynamic mode, reported in the literature.

Sensing Mechanism

SnO₂ was used as a gas sensor-based material that has the ability to sense reducing gases such as H₂. In the atmosphere, the surface of the SnO₂ film interacts with the oxygen molecules in the air. The adsorbed oxygen molecules form O⁻, O⁻², and O₂⁻ moieties, resulting in the formation of depletion layers at the surface of the SnO₂ film (Chang, 1980). As a result, the SnO₂ becomes more resistive (due to lack of electrons in the film conduction band). **Figure 8A** describes the resulting band bending and the formation of the electron barrier at the SnO₂ film surface. In the presence of H₂, the H₂ molecules capture the oxygen moieties and release electrons back into the conduction band of the SnO₂ thin film, therefore decreasing its resistance. This process is described by the following equation:



The enhanced gas-sensing performances of the AgNPs/SnO₂ sensor can be explained by the electronic sensitization mechanism, which is based on the controlled carrier concentration (Yamazoe et al., 1983). The surface region of Ag nanoparticles contains two oxidation states Ag⁰ and Ag⁺ (Ag₂O), as confirmed by the XPS analysis. This mixture leads to the production of the redox couple Ag⁺/Ag⁰ (Matsushima et al., 1988). The couple has an electronic potential of 5.3 eV (Matsushima et al., 1988). When a contact is formed between Ag

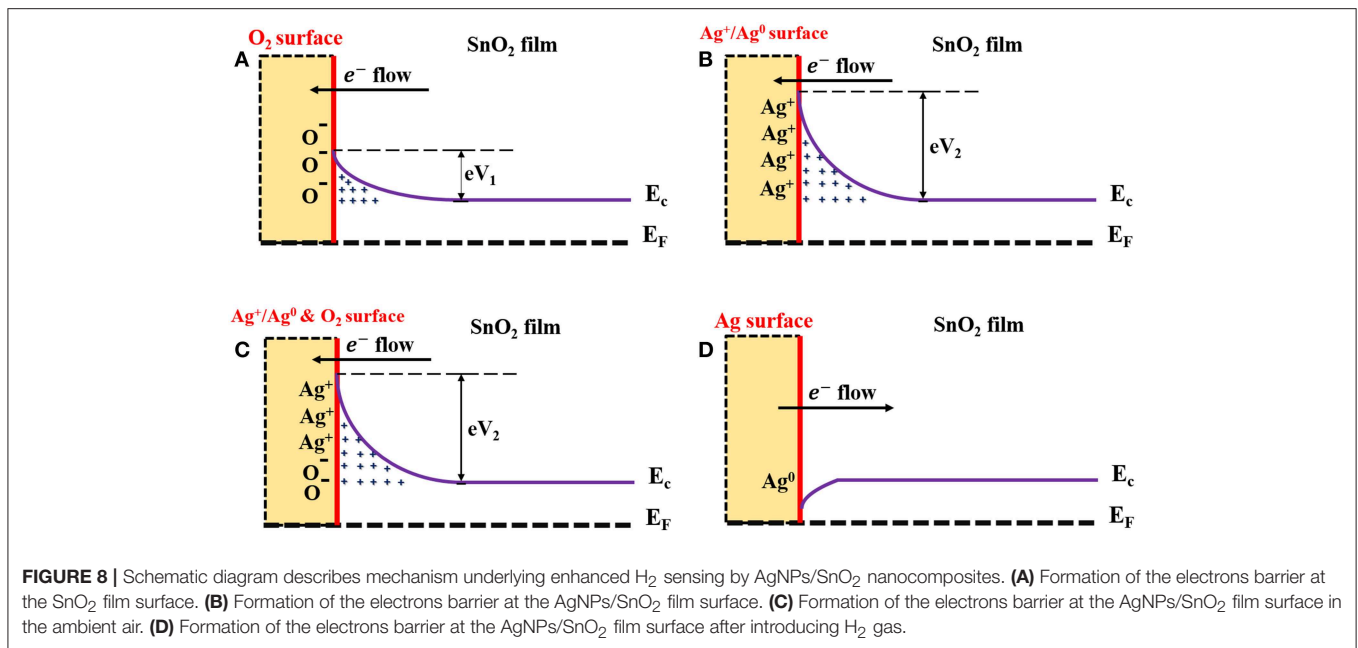


FIGURE 8 | Schematic diagram describes mechanism underlying enhanced H₂ sensing by AgNPs/SnO₂ nanocomposites. **(A)** Formation of the electrons barrier at the SnO₂ film surface. **(B)** Formation of the electrons barrier at the AgNPs/SnO₂ film surface. **(C)** Formation of the electrons barrier at the AgNPs/SnO₂ film surface in the ambient air. **(D)** Formation of the electrons barrier at the AgNPs/SnO₂ film surface after introducing H₂ gas.

NPs and n n-type semiconductor oxide whose electron affinity is <5.3 eV, the Fermi level of the n-type semiconductor is pinned to the Ag⁺/Ag⁰ potential. This leads to the increase of the electron depletion region and to a decrease of the semiconductor oxide conductivity. In our case, the electron affinity (Φ_s) of the SnO₂ is 4.60 eV (Li et al., 2016). Therefore, the Fermi level of the SnO₂ becomes aligned with the work function and electron affinity of Ag⁰ and Ag⁺, respectively. As a result of electron flows from the SnO₂ surface, the energy bands of the SnO₂ will bend downward to reach the equilibrium level with the energy of the Ag⁺/Ag⁰, and hence, the AgNPs/SnO₂ film will have a higher resistance than that of pure SnO₂ as shown in **Figure 8B**. The electron barrier at the surface of the SnO₂ film now depends on the energy of the barriers eV₁ and eV₂, which result from oxygen adsorption and Ag decoration, respectively, as in **Figure 8C**. Nevertheless, the significance conurbation would be from the larger energy eV₂. Now, when H₂ is introduced, and following the same mechanism mentioned above as a result of oxygen removal, the Ag₂O changes into metallic Ag, which has a work function of Φ_{Ag} 4.33 (Luth, 1993). Consequently, the energy bends upward to reach the level of the metallic Ag Fermi energy as a result of restoring electrons from Ag to SnO₂ surface as described in **Figure 8D**. Thus, the resistance of the SnO₂ film is more significantly decreased as an indication of H₂ presence.

CONCLUSION

Pristine and post-annealed SnO₂ thin films as well as silver-decorated SnO₂ thin films were fabricated using the DC/RF sputtering system. The structural, morphological, and compositional properties of the as-deposited SnO₂, annealed

SnO₂, and AgNPs/SnO₂ were studied by various characterization techniques. The gas sensing properties of the silver-decorated tin oxide film were tested at different operating temperatures (RT to 500°C), and with varying H₂ concentration (50 to 1,800 ppm), in order to investigate the sensor sensitivity effect. It was found that the addition of the Ag nanoparticles has significantly increased the sensitivity by 67% compared with annealed SnO₂ at 500°C operation temperature. The observed improvement in H₂ sensing was explained according to an electronic sensitization mechanism.

DATA AVAILABILITY

All datasets generated for this study are included in the manuscript/supplementary files.

AUTHOR CONTRIBUTIONS

AM took the measurements, analyzed the data, contributed to the writing of the manuscript, synthesized the films, characterized the materials, and evaluated the sensors. QD designed the experiment, characterized the materials, evaluated the sensors, synthesized the films, and contributed to the writing of the manuscript. ZY designed the experiment, analyzed the data, and contributed to the editing of the manuscript.

ACKNOWLEDGMENTS

Center of Excellence in Nanotechnology (CENT) and the Physics department at King Fahd University of Petroleum and Minerals (KFUPM) are acknowledged for their support.

REFERENCES

- Ansari, S. G., Boroojerdian, P., Sainkar, S. R., Karekar, R. N., Aiyer, R. C., and Kulkarni, S. K. (1997). Grain size effects on H₂ gas sensitivity of thick film resistor using SnO₂ nanoparticles. *Thin Solid Films* 295, 271–276. doi: 10.1016/S0040-6090(96)09152-3
- Chakraborty, R., Dey, A., and Mukhopadhyay, A. K. (2010). Loading rate effect on nanohardness of soda-lime-silica glass. *Metall. Mater. Trans. A* 41, 1301–1312. doi: 10.1007/s11661-010-0176-8
- Chang, S. C. (1980). Oxygen chemisorption on tin oxide: correlation between electrical conductivity and EPR measurements. *J. Vac. Sci. Technol.* 17, 366–369. doi: 10.1116/1.570389
- Chen, X., Guo, Z., Xu, W. H., Yao, H. B., Li, M. Q., Liu, J. H., et al. (2011). Templating synthesis of SnO₂ nanotubes loaded with Ag₂O nanoparticles and their enhanced gas sensing properties. *Adv. Funct. Mater.* 21, 2049–2056. doi: 10.1002/adfm.201002701
- Cho, S. (2014). Effect of growth temperature on structural, electrical, and optical properties of Gd-doped zinc oxide films. *Phys. Status Solidi A Appl. Res.* 211, 709–713. doi: 10.1002/pssa.201330345
- Crabtree, G. W., Dresselhaus, M. S., and Buchanan, M. V. (2004). The hydrogen economy. *Phys. Today* 57, 39–44. doi: 10.1063/1.1878333
- D'amico, A., Palma, A., and Verona, E. (1982). Surface acoustic wave hydrogen sensor. *Sens. Actuators* 3, 31–39. doi: 10.1016/0250-6874(82)80004-8
- Dasgupta, N. P., Neubert, S., Lee, W., Trejo, O., Lee, J. R., and Prinz, F. B. (2010). Atomic layer deposition of Al-doped ZnO films: effect of grain orientation on conductivity. *Chem. Mater.* 22, 4769–4775. doi: 10.1021/cm101227h
- Deivasegamani, R., Karunanidhi, G., Santhosh, C., Gopal, T., Neogi, A., Nivetha, R., et al. (2017). Chemoresistive sensor for hydrogen using thin films of tin dioxide doped with cerium and palladium. *Microchim. Acta* 184, 4765–4773. doi: 10.1007/s00604-017-2514-7
- Drmosh, Q. A., Hossain, M. K., Alharbi, F. H., and Tabet, N. (2015). Morphological, structural and optical properties of silver treated zinc oxide thin film. *J. Mater. Sci-Mater. El.* 26, 139–148. doi: 10.1007/s10854-014-2375-3
- El-Maghraby, E. M., Qurashi, A., and Yamazaki, T. (2013). Synthesis of SnO₂ nanowires their structural and H₂ gas sensing properties. *Ceram. Int.* 39, 8475–8480. doi: 10.1016/j.ceramint.2013.01.112
- Hwang, I. S., Choi, J. K., Woo, H. S., Kim, S. J., Jung, S. Y., Seong, T. Y., et al. (2011). Facile control of C₂H₅OH sensing characteristics by decorating discrete Ag nanoclusters on SnO₂ nanowire networks. *ACS Appl. Mater. Interfaces* 3, 3140–3145. doi: 10.1021/am200647f
- Ippolito, S. J., Kandasamy, S., Kalantar-Zadeh, K., and Wlodarski, W. (2005). Hydrogen sensing characteristics of WO₃ thin film conductometric sensors activated by Pt and Au catalysts. *Sens. Actuators B Chem.* 108, 154–158. doi: 10.1016/j.snb.2004.11.092
- Kocemba, I., and Rynkowski, J. (2011). The influence of catalytic activity on the response of Pt/SnO₂ gas sensors to carbon monoxide and hydrogen. *Sens. Actuators B Chem.* 155, 659–666. doi: 10.1016/j.snb.2011.01.026
- Kohl, D. (1990). The role of noble metals in the chemistry of solid-state gas sensors. *Sens. Actuators B Chem.* 1, 158–165. doi: 10.1016/0925-4005(90)80193-4
- Korotcenkov, G., Blinov, I., Ivanov, M., and Stetter, J. R. (2007). Ozone sensors on the base of SnO₂ films deposited by spray pyrolysis. *Sens. Actuators B Chem.* 120, 679–686. doi: 10.1016/j.snb.2006.03.029
- Kumar, V., Sharma, S. K., Sharma, T. P., and Singh, V. (1999). Band gap determination in thick films from reflectance measurements. *Opt. Mater.* 12, 115–119. doi: 10.1016/S0925-3467(98)00052-4
- Li, H. H., He, Y., Jin, P. P., Cao, Y., Fan, M. H., Zou, X., et al. (2016). Highly selective detection of trace hydrogen against CO and CH₄ by Ag/Ag₂O–SnO₂ composite microstructures. *Sens. Actuators B Chem.* 228, 515–522. doi: 10.1016/j.snb.2016.01.078
- Liewhiran, C., Tamaekong, N., Tuantranont, A., Wisitsoraat, A., and Phanichphant, S. (2014). The effect of Pt nanoparticles loading on H₂ sensing properties of flame-spray-made SnO₂ sensing films. *Mater. Chem. Phys.* 147, 661–672. doi: 10.1016/j.matchemphys.2014.06.005
- Lippke, G. M. G., Singh, S., and Hoehn, R. K. (2018). *Staged Hydrotreating and Hydrocracking Process and Apparatus*. United States Patent Application No. US20180223198A1.
- Luth, H. (1993). *Surfaces and Interfaces of Solids*. Berlin: Springer. doi: 10.1007/978-3-662-10159-9
- Majumdar, S., Nag, P., and Devi, P. S. (2014). Enhanced performance of CNT/SnO₂ thick film gas sensors towards hydrogen. *Mater. Chem. Phys.* 147, 79–85. doi: 10.1016/j.matchemphys.2014.04.009
- Matsushima, S., Teraoka, Y., Miura, N., and Yamazoe, N. (1988). Electronic interaction between metal additives and tin dioxide in tin dioxide-based gas sensors. *Jpn. J. Appl. Phys.* 27:1798. doi: 10.1143/JJAP.27.1798
- Moseley, P. T. (1997). Solid state gas sensors. *Meas. Sci. Technol.* 8, 223–237. doi: 10.1088/0957-0233/8/3/003
- Pal, A., and Agarwal, A. K. (2018). “Hydrogen for internal combustion engines,” in *Prospects of Alternative Transportation Fuels* (Singapore: Springer), 39–54. doi: 10.1007/978-981-10-7518-6_4
- Reddy, A. S., Figueiredo, N. M., and Cavaleiro, A. (2013). Nanocrystalline Au: Ag: SnO₂ films prepared by pulsed magnetron sputtering. *J. Phys. Chem. Solids* 74, 825–829. doi: 10.1016/j.jpcs.2013.01.023
- Ren, H., Gu, C., Joo, S. W., Cui, J., Sun, Y., and Huang, J. (2018). Preparation of SnO₂ nanorods on reduced graphene oxide and sensing properties of as-grown nanocomposites towards hydrogen at low working temperature. *Mater. Express* 8, 263–271. doi: 10.1166/mex.2018.1428
- Shen, Y., Wang, W., Fan, A., Wei, D., Liu, W., Han, C., et al. (2015). Highly sensitive hydrogen sensors based on SnO₂ nanomaterials with different morphologies. *Int. J. Hydrogen Energy* 40, 15773–15779. doi: 10.1016/j.ijhydene.2015.09.077
- Shinde, V. R., Lokhande, C. D., Mane, R. S., and Han, S. H. (2005). Hydrophobic and textured ZnO films deposited by chemical bath deposition: annealing effect. *Appl. Surf. Sci.* 245, 407–413. doi: 10.1016/j.apsusc.2004.10.036
- Singh, G., and Singh, R. C. (2019). Highly sensitive gas sensor based on Er-doped SnO₂ nanostructures and its temperature dependent selectivity towards hydrogen and ethanol. *Sens. Actuators B Chem.* 282, 373–383. doi: 10.1016/j.snb.2018.11.086
- Sonwane, N. D., Maity, M. D., and Kondawar, S. B. (2019). Conducting polyaniline/SnO₂ nanocomposite for room temperature hydrogen gas sensing. *Mater. Today* 15, 447–453. doi: 10.1016/j.matpr.2019.04.106
- Tsujimura, T., and Suzuki, Y. (2019). Development of a large-sized direct injection hydrogen engine for a stationary power generator. *Int. J. Hydrogen Energy* 44, 11355–11369. doi: 10.1016/j.ijhydene.2018.09.178
- Van Duy, N., Hoa, N. D., and Van Hieu, N. (2012). Effective hydrogen gas nanosensor based on bead-like nanowires of platinum-decorated tin oxide. *Sens. Actuators B Chem.* 173, 211–217. doi: 10.1016/j.snb.2012.06.079
- Wang, L., Li, J., Wang, Y., Yu, K., Tang, X., Zhang, Y., et al. (2016). Construction of 1D SnO₂-coated ZnO nanowire heterojunction for their improved n-butylamine sensing performances. *Sci. Rep.* 6:35079. doi: 10.1038/srep35079
- Wang, Y., Ma, J., Ji, F., Yu, X., and Ma, H. (2005). Structural and photoluminescence characters of SnO₂: Sb films deposited by RF magnetron sputtering. *J. Lumin.* 114, 71–76. doi: 10.1016/j.jlumin.2004.12.003
- Wu, B., Zhao, C., Xu, B., and Li, Y. (2018). Optical fiber hydrogen sensor with single Sagnac interferometer loop based on Vernier effect. *Sens. Actuators B Chem.* 255, 3011–3016. doi: 10.1016/j.snb.2017.09.124
- Wu, R. J., Lin, D. J., Yu, M. R., Chen, M. H., and Lai, H. F. (2013). Ag@ SnO₂ core-shell material for use in fast-response ethanol sensor at room operating temperature. *Sens. Actuators B Chem.* 178, 185–191. doi: 10.1016/j.snb.2012.12.052
- Yamazoe, N., Kurokawa, Y., and Seiyama, T. (1983). Effects of additives on semiconductor gas sensors. *Sens. Actuators* 4, 283–289. doi: 10.1016/0250-6874(83)85034-3
- Yang, L., Yin, C., Zhang, Z., and Zhu, B. (2014). A study of hydrogen sensing properties and microstructure for highly dispersed Pd SnO₂ thin films with high response magnitude. *Appl. Surf. Sci.* 311, 74–82. doi: 10.1016/j.apsusc.2014.05.003
- Zhang, D., Jiang, C., and Zhang, Y. (2017). Room temperature hydrogen gas sensor based on palladium decorated tin oxide/molybdenum disulfide

- ternary hybrid via hydrothermal route. *Sens. Actuators B Chem.* 242, 15–24. doi: 10.1016/j.snb.2016.11.005
- Zhang, Z., Yin, C., Yang, L., Jiang, J., and Guo, Y. (2019). Optimizing the gas sensing characteristics of Co-doped SnO₂ thin film based hydrogen sensor. *J. Alloys Compd.* 785, 819–825. doi: 10.1016/j.jallcom.2019.01.244
- Zielinska, A., Kowalska, E., Sobczak, J. W., Łacka, I., Gazda, M., Ohtani, B., et al. (2010). Silver-doped TiO₂ prepared by microemulsion method: surface properties, bio- and photoactivity. *Sep. Purif. Technol.* 72, 309–318. doi: 10.1016/j.seppur.2010.03.002

Conflict of Interest Statement: The authors declare that the research was conducted in the absence of any commercial or financial relationships that could be construed as a potential conflict of interest.

Copyright © 2019 Mohamedkhair, Drmsh and Yamani. This is an open-access article distributed under the terms of the Creative Commons Attribution License (CC BY). The use, distribution or reproduction in other forums is permitted, provided the original author(s) and the copyright owner(s) are credited and that the original publication in this journal is cited, in accordance with accepted academic practice. No use, distribution or reproduction is permitted which does not comply with these terms.